

Effect of Aluminum Doping on some physical Properties of TiO₂ Thin Films Prepared by Chemical Spray Method

همسة عبد الكريم حمود

المديرية العامة للتربية في محافظة بغداد/ الرصافة الثالثة

E-mail: erth.mn123@yahoo.com

الملخص:

يعرض البحث تأثير التشويب بالألمنيوم على اوكسيد التيتانيوم المحضر بطريقة التحلل الكيميائي الحراري على قواعد من الزجاج وبتراكيز مختلفة من شائبة الألمنيوم (٠، ١، ٣) %، وتم استخدام تقنيات مجهر القوى الذرية، حيود الاشعة السينية والمطياف البصري/ فوق البنفسجي لدراسة هذه الاغشية، تم فحص طوبوغرافية السطح المتأثرة بالتشويب بالألمنيوم، تم فحص الخصائص التركيبية والخواص البصرية ، فإن زيادة تركيز التشويب بالألمنيوم (٠ إلى ٣ %) يزيد من حجم الحبيبي حتى يصل إلى قيمته الأعلى عند التشويب بنسبة ٣ % من الألمنيوم . بينما قلت قيمة فجوة الطاقة من ٣.٣٦ إلى ٣.٢٤ فولت، اغشية اوكسيد التيتانيوم الرقيقة لديها معامل انكسار ومعامل خمود منخفض مع زيادة التشويب بالألمنيوم، وفقاً للتجارب البصرية.

الكلمات المفتاحية: التحلل الكيميائي الحراري، أغشية Al: TiO₂، الخصائص التركيبية و البصرية.

Abstract

The effect of doping aluminum (Al) into Titanium dioxide (TiO₂) on glass substrates coated by Chemical spray pyrolysis (CSP) utilizing different doping concentrations, namely 0wt. percent Al, 1wt. percent Al, and 3wt. percent Al, was investigated. Using tools such as an atomic force microscope (AFM), an X-ray diffractometer (XRD), and an ultraviolet-visible spectrometer, Surface topologies affected by Al doping, structural characteristics, and optical properties were examined (UV-Vis). increasing aluminum dopant concentration (0 to 3 mol%)

increases the crystallite size until it reaches its maximum value at 3 mol% aluminum. The band gap, on the other hand, shrinks from 3.36 to 3.24 eV. TiO₂ thin films have a decreasing refractive index and extinction coefficient as the Al doping level increases, according to optical experiments.

Keywords: CSM, TiO₂: Al thin film, morphology and Optical properties.

Introduction

The band gap TiO₂ is very large (3.2 eV–3.5 eV), so it can only absorb UV spectrum, Accounting for 3–5% of solar irradiation [1]. Rutile, anatase, brookite, and srilankite are the four known structures of (TiO₂) at ambient circumstances (TiO₂-II). The most stable structure is rutile [2–4]. Single crystals, powders, ceramics, and thin films can all be made from TiO₂. Transition metal oxides are frequently nonstoichiometric, and oxygen vacancies are the most common defect in TiO₂ at near-atmospheric oxygen pressure. The lack of oxygen causes an overabundance of electrons to be introduced into the substance, resulting in an increase in electrical conductivity [5]. TiO_{2-x} is an n-type semiconductor because the oxygen vacancies operate as electron donors, as opposed to p-type semiconductors, which contain electron acceptors. [6] As a result, numerous attempts were undertaken to either manage the oxygen vacancy content or inject charge carriers (doping) into TiO₂ to improve or reduce electrical conductivity, depending on the intended use [7–11]. The selection of doping material plays a vital role in the improvement of TiO₂ lattice. The dopant material should have same ionic radii as the TiO₂ lattice. Copper (Cu), zinc (Zn) and aluminum (Al) cause more effective doping with TiO₂ thin films electrode since ionic radius of these are similar to that of TiO₂. The

ionic radius of Cu^{2+} , Zn^{2+} and Al^{3+} is 0.87\AA , 0.88\AA and 0.68\AA respectively while Ti^{4+} is 0.60\AA . Hence Cu^{2+} , Zn^{2+} and by substituting Al^{3+} ion in TiO_2 lattice, TiO_2 can be stabilized in anatase phase without losing its crystal structure [12, 13]. Sputtering [14], e-beam evaporation. [15], CVD [16], sol-gel technique. [17], PLD [18], electrodeposition. [19], hydrothermal [20], and CSP [21] have all been utilized to produce TiO_2 thin films. In this study, a spray pyrolysis approach was used to develop TiO_2 and Al doped TiO_2 thin films over glass substrates, and structural, surface morphological, and optical characteristics were studied in detail. The oxygen vacancy concentration will rise in this situation, and the electron concentration will fall as a result. Aluminum atoms are acceptor impurities in this case [22]. Spray pyrolysis is a low-cost and convenient method for creating semiconductor thin films. The basic idea of spray pyrolysis is the pyrolytic (endothermic) breakdown of salts of the desired substance to be sprayed onto a substrate kept at a higher temperature, resulting in an individual crystal or group of crystallites. It can produce high-quality, large-area adhesive films with consistent thickness. Varying the spray settings allows for easy control of the deposition rate and film thickness. Doping is simple with this process and maybe done with any ingredient in any quantity by just adding it to the spray solution in any way.

Methodology

The TiO_2 thin films were made by dissolving 0.1 M TiCl_2 (provided by Sigma-Aldrich – Germany) in a 1:1 deionized water and ethanol solution. Al trichloride (AlCl_3) was used as a doping agent It is mixed with deionized water and then adding a few drops of HCl makes the solution transparent (provided by Pub. Chem. India). Al-doped TiO_2

coating was formed on a glass slide substrate by chemical spray pyrolysis. Substrate temperature was 400°C, 28 cm separated the nozzle from the substrate, the spraying time was 8 seconds but extended by 60 seconds to avoid cooling, the spray rate was 4ml/min, and N₂ was utilized as a carrier gas. The layer thickness was determined to be 330 25 nm using the gravimetric technique. XRD was used to determine the structural characteristics. AFM (AA3000 Scanning Probe Microscope) was employed to study surface of the deposited films. UV-Visible spectrophotometer was employed for recording spectra of absorption in the 300–900 nm wavelength range.

Characterization

Structural Study

In order to determine crystallinity. Figure 1. Depicts The observed XRD patterns of all Al-TiO₂ thin films well matched with standard JCPDS File No: (46-1238). Characteristic peak patterns were corresponding to TiO₂, which was a major anatase phase when undoped with Al. The TiO₂ phase shows three dominant peaks at 23.68°, 24.88°, 33.16°, 33.16° and 67.19° attributed to the (201), (110), (310), (601) and (023) planes respectively. There were no peaks connected to Al or Al₂O₃, suggesting that Al isn't producing a major second phase [23]. diffraction pattern indicated that they were produced from single phase orthorhombic brookite TiO₂. The TiO₂ peaks increase slightly with the increasing the Al doping concentration due to the disorder caused by the size of ionic radius Al³⁺ and Ti⁴⁺ [23, 24]. It is found that the size of the particle increases slightly in all films with higher concentration values and results are consistent with the AFM results. The increasing crystallizing of the sample attribute to annealed

films with synthesis causes significant dominant peaks of TiO₂ films. Crystallite size was calculated using Scherrer's formula [25]:

$$D = \frac{k\lambda}{\beta \cos\theta} \quad \text{--- -- 1}$$

Where; k = 0.9 is shape factor, k is Used wavelenghts (1.5405Å), β is FWHM, and θ is the Bragg's angle. Calculation of the average crystallite size based on XRD peaks (110) with 2θ=24.88° at different doping was found to be 11.93 nm. Information about the crystal structure can be obtained from the dislocation density of the crystal.

The density of dislocations was determined employing the formula: [26]:

$$\delta = \frac{1}{D^2} \quad \text{--- -- (2)}$$

A low dislocation density will result in a faster crystallization. A dislocation is a flaw in a crystal caused by misregistration of the lattice in one area of the crystal compared to other. δ is a metric for measuring lattice flaws and faults.

In order to calculate strain (ε) and dislocation density (d), we use the following equations [27]:

$$\varepsilon = \frac{\beta \cos\theta}{4} \quad \text{--- -- (3)}$$

Crystallite size increases as strain and dislocation density decrease, as shown in Table 1, indicating improved crystallinity with increased Al doping. Crystallite sizes increase as strain and dislocation densities decrease, indicating impurities, flaws, and lattice distortion in the film [28].

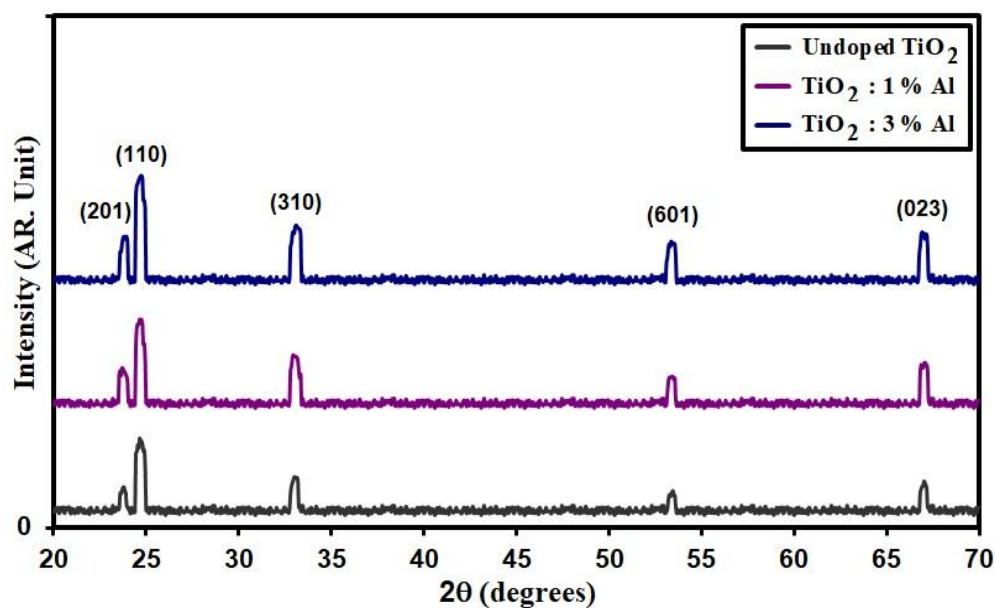


Fig. 1. XRD patterns of TiO_2 :Al films are undoped.

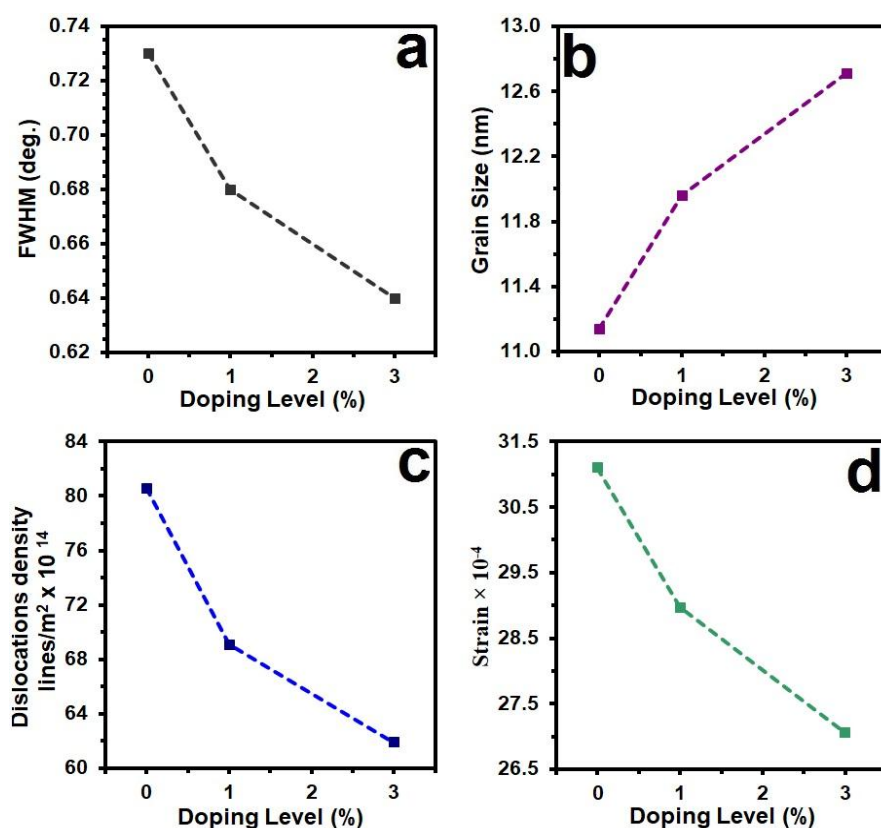


Fig. 2. X-ray parameter of pure and TiO_2 :Al films.

Table 1. Microstructural TiO_2 : Al films and their parameters

Specimen	2θ ($^{\circ}$)	(hkl) Plane	FWHM ($^{\circ}$)	Optical bandgap (eV)	Grain size (nm)	Dislocations density ($\times 10^{14}$) (lines/m ²)	Strain ($\times 10^{-4}$)
Undoped TiO ₂	24.88	110	0.73	3.36	11.14	80.58	31.10
TiO ₂ : 1% Al	24.85	110	0.68	3.30	11.96	69.09	28.97
TiO ₂ : 3% Al	24.82	110	0.64	3.24	12.71	61.90	27.26

AFM Study

An AFM was used to study the topography of entended films. In Figure 3, it gives the AFM image of the undoped and TiO₂:Al histograms of distribution of grain sizes on the surface, which was compared to the AFM image of (Figure 3a1, 3b1 and 3c1). About 5.39 nm of roughness is measured on the TiO₂ surface. The AFM image reveals the polycrystalline film to have the same grain size, as established by XRD measurements. The sizes of TiO₂ grains reach the nanometer scale. AFM investigation shows the three dimensions image and the average particle size in nanometer dimension and There are no cracks in any of the deposits and the films are not compacted and uniform distribution. Table 2 illustrates the AFM information for all films. AFM data demonstrate the surface roughness and morphology and the differences between the types of concentration. The average diameter, average roughness and average RMS plot of pure and TiO₂:Al films

demonstrates the values reduced when the Al content increases. As a result of the doping of TiO₂ with Al, smaller grains are present on the surface [29] is the reason for this.

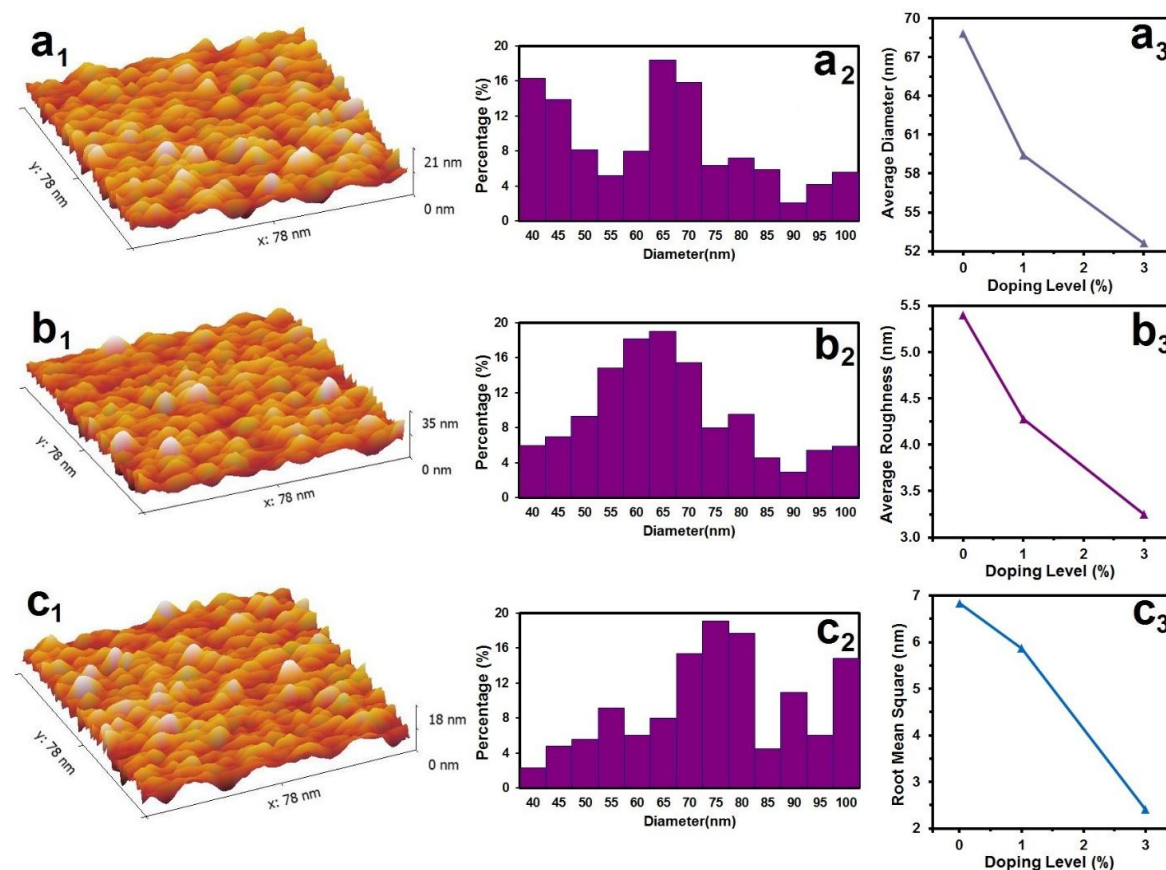


Fig.3. AFM of pure and TiO₂:Al films.

Table 2. AFM parameter measurement of pure and TiO₂:Al films.

Samples	Average size nm	Particle R _a (nm)	R. M. S. (nm)
Undoped TiO ₂	68.83	5.39	6.84
TiO ₂ : 1% Al	59.42	4.28	5.87

Fig.4. Transmittance of pure and TiO₂:Al films with different dopant.

Equation (4) is used to calculate the optical absorption coefficient [30]:

$$\alpha = \frac{1}{d} \ln\left(\frac{1}{T}\right) \quad \text{--- (4)}$$

T represents optical transmittance, and d represents thickness of film. Figure 5 the absorption coefficient of undoped TiO₂ shifted to lower photon energies after Al doping. It is well known that doping improves TiO₂'s absorbance spectrum. The introduction of a metal dopant into the TiO₂ matrix can result in the formation of a new energy level in TiO₂ bandgap. As a result, the amount of photon energy required to activate an electron decreases, raising the vis absorbance value [31].

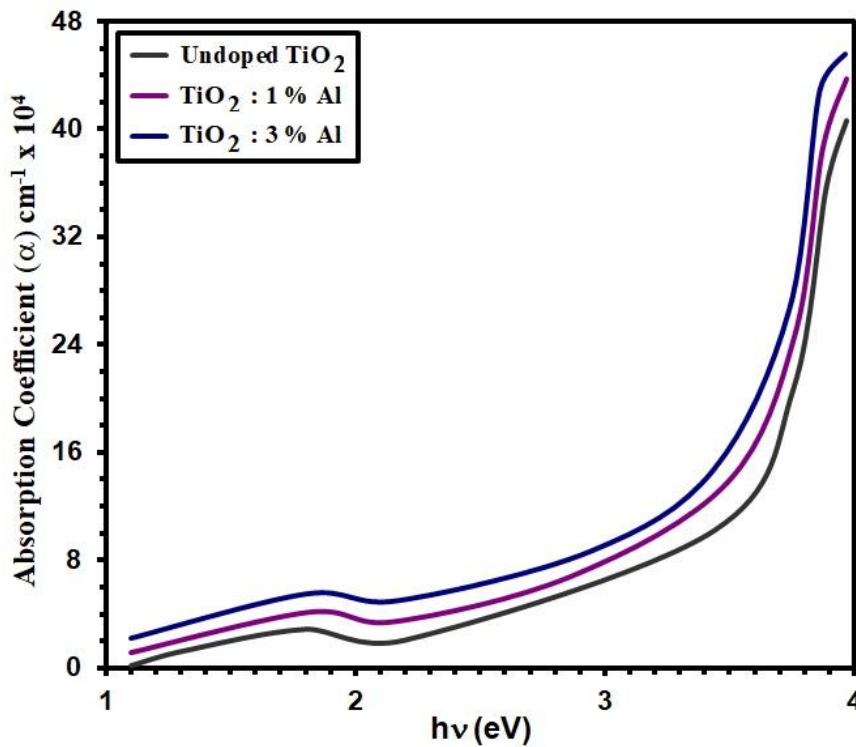


Fig. 5. α of pure and TiO₂:Al films with different dopant.

As a function of optical band gap, optical absorption coefficient is given by equation [30]:

$$\alpha h\nu = A(h\nu - E_g)^n \quad \text{--- --- --- (5)}$$

A band gap is defined as E_g , A represents a constant, and n denotes the type of the transitions [32].

The fluctuation of $(\alpha h\nu)^2$ versus photon energy ($h\nu$) is seen in Figure 6. Extrapolation of the linear component of this curve yields the band gap energy values (E_g). Figure 6 depicts the relationship between E_g values and the quantity of Al doping.

Pure TiO_2 and 3% Al doped TiO_2 have energy band gaps of 3.36eV and 3.25eV, respectively, In the case of doped TiO_2 , this leads to a shift in the uv-vis spectrum towards lower wavelength region due to which absorption is increased as compared to pure TiO_2 . UV-Vis diffuse reflectance spectra of Al doped TiO_2 , As a result of Kubelka-Munk function [33].

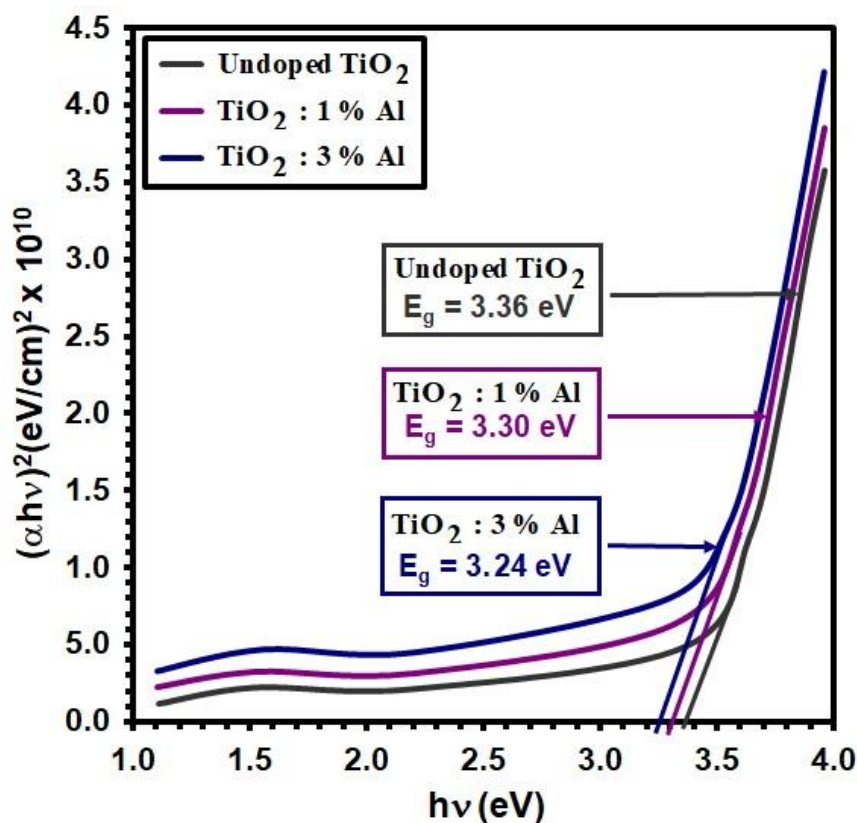


Fig.6. direct band gap (E_g) of pure and TiO_2 :Al films with different dopant.

The extinction coefficient may be calculated using the following formula [34]:

$$k = \frac{\alpha \lambda}{4\pi} \quad \text{--- (5)}$$

Where (λ) is the wavelength of the incident radiation impinging on the film. Extinction coefficient k versus wavelength spectra is shown in Fig. 7

from the reflectance (R) data, The refractive index (n) can be determined using the relation [35]:

$$R = \frac{(n - 1)^2}{(n + 1)^2} \quad \text{--- --- (6)}$$

Figure 8 shows the refractive index (n) against wavelength spectrum.

With increasing Al content, a function of wavelength drops for refractive index (n) and extinction coefficient (k). The refractive index of a film is proportional to its atom density and crystallinity; as crystallite size increases, the refractive index decreases [36]. The modest drop in the extinction coefficient might be attributable to light absorption [37].

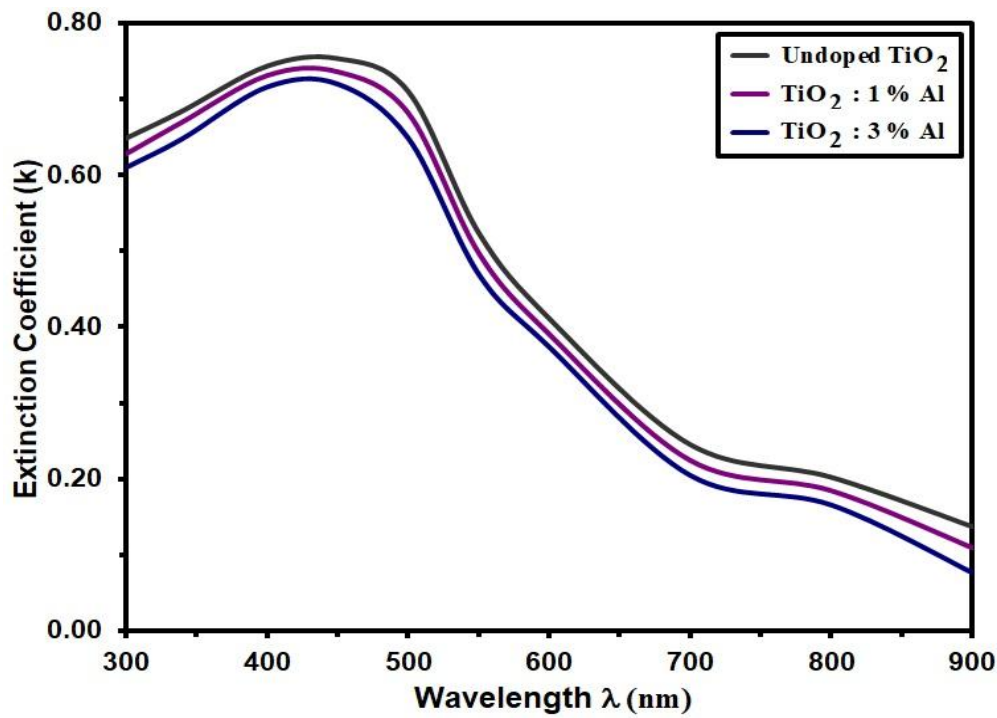


Fig.7. k of pure and TiO₂:Al films with different dopant.

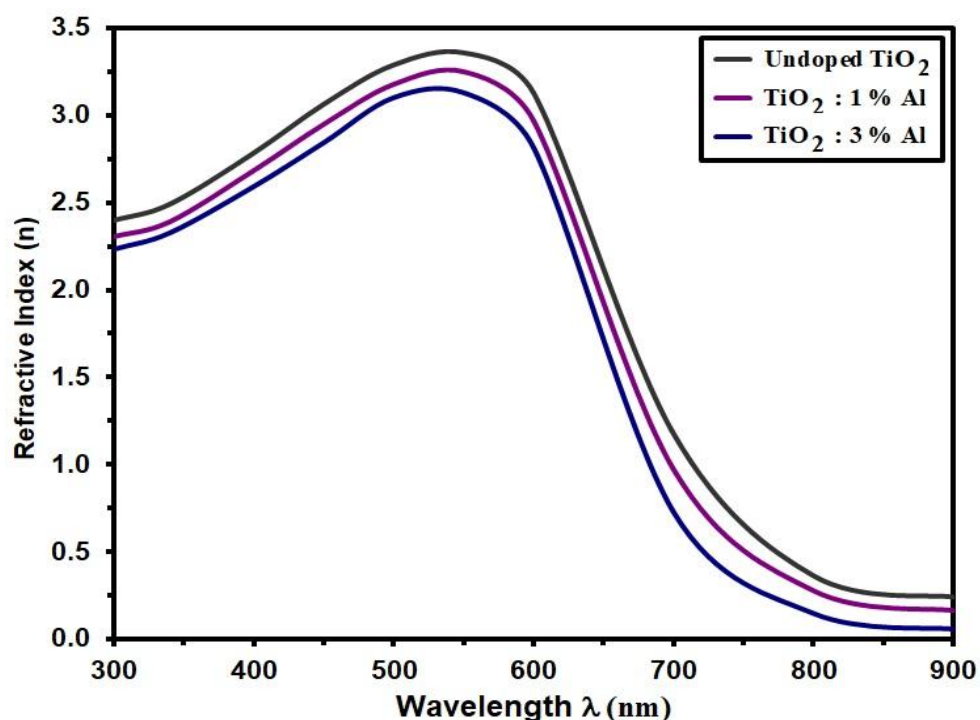


Fig. 8. n of pure and TiO_2 : Al films with different dopant.

Conclusion

Spray pyrolysis at 400°C was used to successfully synthesize Al doped TiO_2 thin films on glass substrate. The impact of aluminum dopant on structural, surface topologies, and optical characteristics have been investigated. The films are polycrystalline with a brookite crystal phase, according to XRD measurements. UV-Vis experiments show that increasing the Al content reduces the transmitted spectrum and refractive index of TiO_2 thin films. Furthermore, increasing the Al concentration causes a blue shift in the optical band gap energy of TiO_2 thin films, which lowers from 3.36 to 3.24 eV. Increased Al dopant levels reduce surface roughness and grain size, according to AFM research.

References

- [1] A. V. Emeline, V. N. Kuznetsov, V. K. Rybchuk, N. Serpone, Visible–Light–Active Titania Photocatalysts: The Case of N–Doped TiO_{2s} Properties and Some Fundamental Issues, International Journal of Photoenergy,19 (2008).
- [2] R. W. G. Wyckoff: “Crystal structure”, Interscience Publishers, New York (1965).
- [3] R. K. Linde and P. S. DeCarli, The Journal of Chemical Physics 50 (1969), 319.
- [4] J. Haines and J. N. Léger, Physica B 192 (1993), 233.
- [5] P. Kofstad: “Nonstoichiometry, diffusion, and electrical conductivity in binary metal oxides”, Wiley Interscience, New York (1972).
- [6] S. M. Sze: “Physics of semiconductor devices”, Wiley Interscience, New York (1981).
- [7] G. H. Johnson, Journal of The American Ceramic Society 36 (1953), 97.
- [8] J. F. Houlihan, J. R. Hamilton, and D. P. Madacsi, Material Research Bulletin 14 (1979), 915.
- [9] N. G. Eror, Journal of Solid State Chemistry 38 (1981), 281.
- [10] K. Tennakone, S. W. M. S. Wickramanayake, P. Samarasekara, and C. A. N. Fernando, Physica Status Solidi (a) 104 (1987), K57.
- [11] S. R. Kurtz and R. G. Gordon, Thin Solid Films 147 (1987), 167.
- [12] J. E. Lee, S. Oh, and D. Park, Thin Solid Films 457, 230 (2004).
- [13] U. Gesenhues, J. Photochem. Photobiol. A 139, 243 (2001).

- [14] R.V. Alvarado, A.P. de la Beneitez, R.L. Callejas, J. Physics, Conf. Series. 591, 012042 (2015).
- [15] M.H. Mangrola, V.G. Joshi, Mater. Today: Proc. 4, 2 (2017).
- [16] S.S. Huang, J.S. Chen, J. Mater. Sci.: Mater. Electron. 13, 77–81(2002).
- [17] N.D. Johari, Z.M. Rosli, J.M. Juoi, J. Mater. Res. Technol. 8, 2(2019).
- [18] C. Garapon, C. Champeaux, J. Mugnier, Appl. Surf. Sci. 96, 836–841 (1996).
- [19] F. C. E. Moursli, A. Douayar, F. Hajji, Sens. Transducers.27, 258–263 (2014).
- [20] T. D. Dongale, S. S. Shinde, R. K. Kamat, J. Alloys Compd. 593, 267–270 (2014).
- [21] V. Tamilnayagam, P. Jegatheesan, K. Pakiyaraj, J. Mater. Sci.: Mater. Electron. 27, 11530–11535 (2016).
- [22] P. Kofstad, “Nonstoichiometry, diffusion, and electrical conductivity in binary metal oxides”, Wiley Interscience, New York (1972).
- [23] Y. J. Choi, Z. Seeley, A. Bandyopadhyay, S. Bose and S. A. Akbar: Sens. Actuators B, 2007, 124B, 111–117.
- [24] W. Zhang, X. Pei, J. Chen and H. He, Mater. Sci. Semicond. Process. 38, 24–30 (2015).
- [25] M. Epifani, A. Helwig, J. Arbiol, R. Diaz, L. Francioso, P. Siciliano, G. Mueller, and J. R. Morante, Sens. Actuators, B 130(2), 599–608 (2008).

[26] P. Malliga, J. Pandiarajan, N. Prithivikumaran, K. Neyvasagam, “Influence of film thickness on structural and optical properties of sol–gel spin coated TiO₂ thin film,” J Appl Phys 6:22–28(2014).

[27] G. B. Williamson, R. C. Smallman, Philos Magn 1:34(1956).

[28] T. P. Rao, M. C. S. Kumar, A. Safarulla, V. Ganesan, S. R. Barman, C. Sanjeeviraja, “Physical properties of ZnO thin films deposited at various substrate temperatures using spray pyrolysis,” Phys B 405:2226–2231(2010).

[29] Masoud Khosravi, Mohammad Reza Toroghinejad, Mohammad Reza Vaezi and Ali Saidi, “Structural, electrical, optical and morphological properties of aluminum doped TiO₂ thin films deposited by spray pyrolysis method,” Journal of Materials Science: Materials in Electronics, (31)9, 7150–7163(2020).

[30] Y. Gao, Y. Masuda, Z. Peng, J. Mater. Chem. 13, 608 (2003).

[31] A. Zaleska: Recent Patents Eng., 2, 157–164(2008).

[32] N.N. Ilkhechi, N. Ghobadi, B.K. Kaleji, Opt. Quant. Electron. 48, 416(2016).

[33] S. Qiu, S. J. kalita, Materials Science and Engineering , 327, 435–436(2006).

[34] J. I, Pankove, “Optical Processes in Semiconductors,” Dover, New York, 93(1971).

[35] P. E Agbo, M. N. Nnabuchi , Chalcogenide Letters 8, 273 (2011).

[36] R. Al Samar, G. Ferblantier, F. Mailly, P. Gall–Borrut and A. Foucaran, “Effect of annealing on the electrical and optical properties of electron evaporated ZnO thin films,” Thin Solid Films 473:49–53(2005).

[37] MR. Islam and J. Podder, "Optical properties of ZnO Nano fibre thin films grown by spray pyrolysis of zinc acetate precursor," J Cryst Res Tech. 44:286-292(2009).